HHS Public Access

Author manuscript

Clin Cancer Res. Author manuscript; available in PMC 2020 April 01.

Published in final edited form as:

Clin Cancer Res. 2019 April 01; 25(7): 2314–2322. doi:10.1158/1078-0432.CCR-18-2276.

Dynamic contrast-enhanced MRI detects responses to stroma-directed therapy in mouse models of pancreatic ductal adenocarcinoma

Jianbo Cao[1,2], **Stephen Pickup**[1], **Cynthia Clendenin**[4,5], **Barbara Blouw**[3], **Hoon Choi**[1], **David Kang**[3], **Mark A. Rosen**[1,5], **Peter J. O'Dwyer**[4,5,*], and **Rong Zhou**[1,5,*]

[1]Department of Radiology, University of Pennsylvania, Philadelphia, PA 19104.

[2]Medical College, Xiamen University, Xiamen, Fujian, 361102, P.R. China.

[3]Halozyme Therapeutics, San Diego, CA 92121.

[4]Pancreatic Cancer Research Center, University of Pennsylvania, Philadelphia, PA 19104.

[5]Abramson Cancer Center, University of Pennsylvania, Philadelphia, PA 19104.

Abstract

Objective—The dense stroma underlies the drug resistance of pancreatic ductal adenocarcinoma (PDA) and has motivated the development of stroma-directed drugs. Our objective is to test the concept that dynamic contrast-enhanced (DCE) MRI using FDA-approved contrast media, an imaging method sensitive to the tumor microenvironment, can detect early responses to stroma-directed drug.

Experimental Design—Imaging studies were performed in three mouse models exhibiting high desmoplastic reactions: the autochthonous PDA in genetically engineered mice (KPC), an orthotopic model in syngeneic mice and a xenograft model of human PDA in athymic mice. An investigational drug, PEGPH20 (pegvorhyaluronidase alfa), which degrades hyaluronan in the stroma of PDA, was injected alone or in combination with gemcitabine.

Results—At 24 hours after a single injection of PEGPH20, K^{trans}, a DCE MRI derived marker that measures how fast a unit volume of contrast media is transferred from capillaries to interstitial space, increased 56% and 50% from baseline in the orthotopic and xenograft tumors respectively, compared to a 4% and 6% *decrease* in vehicle groups (both $P<0.05$). Similarly, after three combined treatments, K^{trans} in KPC mice increased 54% while it decreased 4% in controls treated with gemcitabine alone ($P<0.05$). Consistently, after a single injection of PEGPH20, tumor hyaluronan content assessed by immunohistochemistry, was reduced substantially in all three

[*]**Corresponding authors: Rong Zhou**, John Morgan 198, 3620 Hamilton Walk, Philadelphia, PA 19104, Phone: 215-746-8787, Fax: 215-573-2113, rongzhou@upenn.edu; **Peter J. O'Dwyer**, 3400 Civic Center Blvd, Philadelphia, PA 19104, Phone: 215-662-7606, Fax: 215-573-2113, Peter.O'Dwyer@uphs.upenn.edu.

Author contributions: Concept development and study design: RZ, JC, MAR and PJO. Contribution to animal models and reagents: DK and CC. Data acquisitions & analysis: JC, SP, RZ, HC, BB and CC. Manuscript preparations and editing: JC, SP, MAR, PJO, BB, DK and RZ.

Conflict of interest disclosure statement

None of the authors declare any financial interests that could be perceived as being a conflict of interest.

models while drug delivery (measured by paclitaxel accumulation in tumor) was increased by 2.6-fold.

Conclusion—These data demonstrated a DCE-MRI marker, K^{trans}, can detect early responses to stroma-directed drug and reveal the sustained effect of combination treatment (PEGPH20+ gemcitabine).

Keywords

Pancreatic ductal adenocarcinoma; desmoplastic stroma; hyaluronan; dynamic contrast enhanced (DCE)-MRI; microvasculature

Introduction

Pancreatic ductal adenocarcinoma (PDA) is a highly lethal cancer with a 5-year survival rate of 6% (1). PDA is characterized by a dense, desmoplastic stroma, populated by proliferating pancreatic stellate cells (PSCs), which deposit an extracellular matrix (ECM) including collagen, proteoglycans, and glycosaminoglycans (for example, hyaluronan or hyaluronic acid, HA). Accumulation of HA, which is highly water-absorbing, results in a significant increase in interstitial fluid pressure (IFP) in the tumor. This hydrostatic pressure leads to the collapse of blood and lymph vessels, and ultimately hypo-perfusion of the tumor (2). The high IFP in combination with a reduced blood vessel density defines a unique tumor microenvironment featuring a profound lack of functional perfusion (3). Contrast-enhanced radiological imaging often presents a hypo-enhanced PDA tumor (4,5) in contrast to hyper-enhanced neuroendocrine pancreatic tumors, which are hypervascular. It has been recognized that this unique tumor microenvironment, where both blood flow and permeability of the microvasculature are reduced, with the consequence that the transport of small molecule drugs across the capillaries is hindered, underlies the chemoresistance in PDA (3,6,7). Besides high IFP, the stroma also harbors an immune-suppressive microenvironment (8). Taken together, the stroma plays an important role in the overall resistance of PDA to treatment; therefore, overcoming this “stromal resistance” has motivated the development of stroma-directed interventions. One barrier to the development and clinical implementation of these drugs is the lack of a robust non-invasive marker that can be used to evaluate the pharmacodynamic effect of the drug, identify responsive patients and guide combination strategies.

Dynamic contrast-enhanced (DCE)-MRI is sensitive to the tumor microenvironment, especially to changes in microvascular function i.e., permeability and perfusion; hence it may provide a clinically translatable, quantitative imaging marker to assess responses to stroma-directed therapies. While its utility to assess antiangiogenic therapies has been examined extensively in the clinic (9), the potential of DCE-MRI for stroma-directed therapy has been proposed only in a couple of pilot studies (10,11). Therefore, to allow a thorough evaluation of this new application of DCE-MRI, extensive animal model work is necessary, and detailed analyses should provide mechanistic insight of the imaging marker. We hypothesized that a DCE-MRI-derived quantitative marker of microvascular function, K^{trans}, can detect the early response of the PDA to stroma-specific treatment. In the experimental design, we employed three PDA models including the autochthonous PDA in

genetically engineered mice (GEM), an orthotopic model in syngeneic mice and a xenograft model of human PDA in athymic mice. We used an investigational drug, PEGylated recombinant hyaluronidase PH20 (PEGPH20, generic name as pegvorhyaluronidase alfa), which degrades stromal HA and has shown evidence of efficacy in a randomized, multi-center Phase-2 clinical trial of patients with PDA (HALO-202) (12). We examined the effects of a single PEGPH20 injection and in combination with gemcitabine, an active drug for PDA. We corroborated the imaging results with assessments of tumor hyaluronan level and quantitative measurement of drug delivery to the tumor. Our data demonstrated that a quantitative DCE-MRI marker can sensitively detect early responses of PDA to stroma-directed drug and monitor the sustained effect of combination treatment.

Materials and Methods

Materials

PEGPH20, a polyethylene glycol (PEG)-conjugated recombinant human hyaluronidase enzyme that degrades hyaluronan (8), was provided by Halozyme Therapeutics via an institutional material transfer agreement. It was dissolved 3.5 mg/mL in a vehicle (VEH) made of 10 mM histidine and 130 mM sodium chloride (pH 6.5) and an aliquot was diluted in PBS before injection. Human PDA cell line, BxPC-3, was purchased from American Type Culture Collection (ATCC), was authenticated using the Short Tandem Repeat DNA profiling and was tested to be free of mycroplasma by agar culture and Hoechst DNA staining, and was used within 50 passages. An FDA-approved contrast agent for clinical MRI, MultiHance (Bracco Imaging, Princeton, NJ), was diluted (50x) in saline to 10 mM gadolinium (Gd) for injection in mice.

PDA mouse models

All animal procedures were approved by the institutional animal care and use committee (IACUC) of the University of Pennsylvania. A genetically-engineered mouse model harboring a pancreas-specific Cre allele with p53 and Kras mutations referred to as the KPC mouse (13), was maintained at the Mouse Hospital of Pancreatic Cancer Research Center of our institution. KPC mice of both sexes were used in this study. A cell line, 4662-KPC, established from a KPC tumor (14), was used to generate the orthotopic model by injection of 1.25×10^5 cells into the pancreas of syngeneic C57BL/6 mice (9 weeks old, both sexes, Jackson Lab). A xenograft model was generated in athymic mice (NCR nu/nu, 9 weeks old, both sexes, Charles River) by subcutaneous (subQ) injection of 10-million BxPC-3 cells suspended in 0.1 mL PBS in the hind flank.

DCE-MRI protocol and pharmacokinetic (PK) modeling

MRI studies were performed using a 9.4T DirectDrive® system (Agilent, Palo Alto, CA) interfaced with a 12-cm gradient coil (maximal strength 40 gauss/cm). While under isoflurane anesthesia, the mouse was placed inside a 35-mm ID × 10 cm long quadrature birdcage transceiver coil (M2M, Cleveland, OH). Vital signs including ECG, respiration and core temperature were monitored (SAI Inc, Stonybrook, NY) and the core temperature was maintained at 37±0.2°C by directing warm air into the bore of the magnet. Both T_{10} (the longitudinal relaxation time of the tissue before contrast agent injection) mapping and DCE

series were applied to multiple axial slices (4 to 7): one slice containing the left ventricle (LV) of the heart was used to measure the arterial input function (AIF) from the blood signal while remaining slices were used to span the entire tumor.

T_{10} was mapped for both the blood (in the left ventricle of the heart) and tumor using an ECG-gated inversion recovery technique described previously (15,16). The DCE series was acquired using an ECG-gated saturation recovery technique to effectively suppress the in-flow effect (15,17). After the acquisition of 10 pre-contrast images, 0.2 mL of the contrast agent was injected in 10 seconds at a constant rate via a tail vein catheter connected to a syringe pump (Harvard Apparatus, Holliston, MA) while data acquisition continued until 80 images (for each slice) were obtained. Acquisition parameters include FOV=32 mm, matrix size = 64×64, effective TR= 2 × heart beat ≈ 200 ms, TE= 3 ms, flip angle = 7 degree (for T_{10}) and 90 degrees for DCE series. During DCE acquisition, the radiofrequency pulse sequence timing was recorded on a micro-controller device and the record was used to correct ECG triggering errors during post-processing. The AIF, DCE series and T_{10} maps of the tissue were input to a pharmacokinetic model (15,18) using the least squares methods. Pixel-wise parametric maps of K^{trans} (the rate constant of transferring unit volume of contrast agent from capillaries to interstitial space, min^{-1}), k_{ep} (the rate constant from interstitial space to capillaries, min^{-1}), τ_i (the intracellular water life time, sec) and V_e (extracellular and extravascular volume fraction, %, $V_e = K^{trans}/k_{ep}$) were obtained as modeling output.

Immunostaining

A recombinant hyaluronan-binding probe (HTI-601; Halozyme Therapeutics, San Diego, CA) was applied to paraffin sections of the tumor as described previously (19) and the stained slides were digitized using an Aperio Scanner (Leica Biosystems). The hyaluronan-positive and total pixels were counted in the viable tumor region using the vendor's software (Aperio Positive Pixel Count Algorithm). Four sections per tumor were used to estimate tumor hyaluronan content by % positive pixels.

Quantification of drug (paclitaxel) delivery to the tumor

At 24 h post PEGPH20 (or VEH) treatment, paclitaxel formulated in Cremophor-EL and ethanol followed by dilution in saline was i.v. infused (30 mg/kg) over a 30-min period; two hours after infusion, the mouse was euthanized, and tumor was harvested. Paclitaxel was extracted from the tumor tissue and quantified by HPLC following a published protocol (20). Briefly, tumor tissue was weighed and homogenized in a 10:1 ratio (v/w) of buffer (10 mM Tris, 1mM EDTA, and 10% (v/v) glycerol, pH =7.4) and tissue. The homogenate was extracted with ethyl acetate (1:2 v/v, homogenate/ethyl acetate) and centrifuged for 15 min at 16,000×g. The supernatant was collected, dried under nitrogen, and reconstituted with acetonitrile/water (75:25 v/v). The solution was filtered (0.2 μm) and analyzed on an HPLC (JASCO, Easton, MD) equipped with a VIVA C18 column (5 μm 250×4.6 mm). The paclitaxel content was estimated using a calibration curve and normalized to the tissue weight.

Data and statistical analysis

Data are presented as mean ± standard deviation (SD). Coefficient of variance (CV = SD/mean) was used to evaluate the repeatability of tissue and blood T_{10} measurements. Statistical analyses were performed using Prism 6 (GraphPad, San Diego, CA) or SPSS 22 (IBM, New York, NY). In paired studies, the averaged K^{trans}, k_{ep}, and τ_i value of the tumor measured at baseline and post treatment from the same group of mice were compared using the Wilcoxon signed-rank test. The percent changes relative to baseline were compared between treatment groups using the Mann-Whitney U test. The level of α was set at 0.05 to evaluate significance. The distribution of pixel-wise K^{trans} values of tumors measured at baseline and post-treatment was visualized by histograms that were constructed by calculating frequencies of K^{trans} values in each of the 21 bins: bin #1–20 had a fixed bin width of 0.1 min^{-1} while bin #21 included all K^{trans} >2 min^{-1}.

Results

Following the treatment and imaging schedule in Fig 1A–C, we first evaluated whether MRI can detect an early response to stroma-directed drug. MRI was performed at baseline and 24 h after a single i.v. injection of PEGPH20 (1 mg/kg) or vehicle in mice bearing orthotopic tumor (4662-KPC) or human PDA xenograft. For the orthotopic model, mice were studied at 3–4 weeks after tumor inoculation with mean tumor size of 255 mm^2 (61–630 mm^2) while for the xenograft model, 6–8 weeks after inoculation with mean tumor size 294 mm^2 (range: 133–452 mm^2). To evaluate DCE-MRI responses to PEGPH20 plus gemcitabine, KPC mice were enrolled at 13–27 weeks after birth with mean tumor size 175 mm^2 (50–260 mm^2). KPC mice received PEGPH20 (or vehicle) on day 0, 7, and 14 and gemcitabine (50 mg/kg iv) on day 1, 8 and 15. MRI was performed at baseline and again 1–2 days after the treatment was completed.

K^{trans} responds to single or multiple injections of PEGPH20 and to combination treatments

As shown in Fig 1D, tumor was manually defined on T_{10} map; pixel-wise dynamic MR signal in the tumor was fit into a PK model with the knowledge of input function (AIF) and T_{10} to derive parameter maps including K^{trans}. The sensitivity of K^{trans} was tested by performing DCE-MRI at 24 h after a single injection of PEGPH20: the timing coincided with peak depletion of tumor-HA reported earlier (21). Paired data revealed a consistent increase of K^{trans} in both orthotopic (Fig 2A) and human PDA xenograft model (Fig 2B). In comparison, in most vehicle-treated tumors, K^{trans} remained unchanged or decreased. In average, K^{trans} increased 56% from baseline in the orthotopic tumors, and 50% in the xenograft model ($P < 0.05$ for both models, Fig 2D–E). The rate constant, k_{ep}, also exhibited a large increase after PEGPH20 treatment; however, variations in k_{ep} changes were greater than those in K^{trans}.

To test responses to repeated injections, three mice were injected with PEGPH20 weekly for 3 weeks. The paired K^{trans} values revealed a substantial increase 24 h after PEGPH20 injection from the baseline, while partial recovery (reduction of K^{trans}) was observed between injections (Supplemental Fig 1). The pattern of K^{trans} change is consistent with the reversible degradation of tumor hyaluronan by PEGPH20 (22).

Since stroma-directed drugs are combined with gemcitabine in clinical trials, we further tested whether DCE-MRI can robustly detect changes resulted from combination treatments (Fig 1C). After three treatments of PEGPH20 + gemcitabine, K^{trans} in KPC tumors increased 54% from baseline compared to 4% decrease in vehicle + gemcitabine group (Fig 2C, F), suggesting that PEGPH20+gemcitabine treatments led to a sustained improvement of perfusion. Representative K^{trans} maps at baseline and after PEGPH20 treatment are shown for all three models (Fig 2G–L). The pixel-wise parametric maps allowed assessment of spatial heterogeneity of the K^{trans} value across the tumor before and after treatment.

Changes of K^{trans} distribution in response to PEGPH20 and combined treatment

To gain further insights of how the three models may differ in their intrinsic vascular characteristics and responses to stromal therapy, we analyzed the distribution of K^{trans} values using a histogram approach, where pixel-wise K^{trans} values were pooled from individual tumors in each group. Of the three models at baseline, KPC had the lowest frequency in the lowest bin (0–0.1 min^{-1}) of K^{trans} (Fig 3A–C). In the xenograft model, K^{trans} distribution was relatively narrower and shifted toward the left compared to the other models. These findings revealed distinct microvascular function (i.e., the xenograft has the lowest perfusion/permeability while the KPC model the highest), likely determined by their location (subQ vs. orthotopic) and the nature of tumor development (spontaneous vs. implanted).

In response to a single injection of PEGPH20, the orthotopic model showed a remarkable redistribution of K^{trans} (red), which was right-shifted relative to the baseline (black) or to vehicle treatment (blue). The bins representing relatively high K^{trans} values (0.5–1.1 min^{-1}) whose frequency increased 50% or more from baseline were marked by # in Fig 3A, indicating increased perfusion/permeability in response to treatment. In comparison, K^{trans} redistribution from the xenograft model (Fig 3B) was more limited as there were fewer # marked bins and lower K^{trans} values these bins represent (0.5–0.7 min^{-1}). After three PEGPH20+ Gemcitabine treatments, K^{trans} distribution in KPC tumor exhibited a right-shift, featuring a large increase of K^{trans} in bins ranging from 1.0 to 1.5 min^{-1} and ≥ 2.1 min^{-1} (marked by #, Fig 3C). This data suggests that improvement of microvascular function (K^{trans}) was sustained by stromal intervention combined with gemcitabine.

Repeatability of DCE-MRI protocol

To reduce data variability, we standardized the DCE-MRI protocol, including using constant Gd concentration (10 mM), volume and rate of injection via a syringe pump. Vital signs were maintained at physiological level throughout the imaging session. Consequently, a good reproducibility of the protocol was obtained: longitudinal relaxation time (T_{10}) measured from the blood and tumor in all three models revealed low CV (coefficient of variance = SD/mean) of 9% and 10% respectively at baseline (n=23). However, neither blood nor tumor T_{10} was sensitive to PEGPH20 or combined treatment (supplemental Fig 2A–C). Since the clearance of the contrast media takes time, it is not feasible to perform two DCE-MRI sessions in same day to assess the repeatability of K^{trans}. Therefore, we evaluated the VEH-treated mice in paired-study separated by 24 h (Fig 2A–B). Despite one outlier in

Fig 2A, the mean changes of K^{trans} over 24 h were quite small (4–6%) (Fig 2D–E), suggesting that the K^{trans} measurement is relatively robust.

Immunohistochemistry and quantitative measurement of drug delivery to corroborate imaging findings

In all three models, immunostaining revealed a remarkable accumulation of HA in the tumor of VEH-treated mice and dramatic reduction of HA 24 h after a single injection of PEGPH20 (Fig 4A–F). By counting the % of HA-positive pixels in the viable tumor regions, a significant difference of HA-content was found between PEGPH20 versus VEH treated tumors (Fig 4G). However, the xenograft model has higher HA level than other models after treatment – this is consistent with the lower post-treatment K^{trans} values (mean =0.318/min) compared to orthotopic (mean =0.639/min) and KPC (mean =0.608/min) model (Fig 2A–C), suggesting that this model was less responsive to stromal intervention.

To test whether the increase in K^{trans} (from DCE-MRI) was corroborated by increased drug penetration to the tumor bed, we infused paclitaxel in mice bearing orthotopic PDA at 24 hours after a single injection of PEGPH20 and analyzed tumor tissues by HPLC. Our results demonstrated that PEGPH20 treatment resulted in > 2-fold greater paclitaxel accumulation in the tumor (Fig 5 and supplemental Fig 3), consistent with improved perfusion/permeability revealed by K^{trans} results.

Discussion

The unique tumor microenvironment presented by the fibroinflammatory stroma in PDA not only promotes tumor progression but also underlies resistance to treatment. Conflicting results may reflect the complexity of these interactions, since genetic ablation of stromal fibroblasts or the sonic hedgehog (SHH) pathway appeared to enhance tumor aggressiveness (23). Conversely, reversal of desmoplastic stroma by stroma-directed drugs including PEGPH20, vitamin-D analogs (24), SHH inhibitors (25,26) and CD40 agonist antibody (27) have shown promise to overcome gemcitabine resistance, and to extend the survival of KPC mice. Importantly, evidence from clinical trials of PEGPH20 (12) and CD40 (27) suggests that stroma-directed approaches lead to more effective management of PDA. Strikingly, drugs targeting different stromal components or signals induce similar changes in the microvasculature. For example, PEGPH20 selectively degrades HA in the extracellular matrix (2,21), whereas calcitriol/paricalcitol activates the vitamin-D receptors on pancreatic stellate cells (24,28). Both drugs, however, have been shown to improve microvascular function and penetration of small molecule drugs into the tumor (21,24,28,29). Considering that microvasculature is an integral part of the stroma, the converging effect of stroma-directed drugs is not surprising but suggests that an imaging marker sensitive to microvascular function may have general application for various stroma-directed drugs. To date, most DCE-MRI studies have been applied to assess *antivascular* therapies, which induce a *decrease* in K^{trans} when the tumor responds positively (9,30). In contrast, stroma-directed therapy induced an *increase* in K^{trans}, resulting in a more favorable dynamic range and sensitivity of DCE-MRI in this new application, given that PDA is poorly perfused before treatment.

A major effect of PEGPH20 on tumor stroma is to degrade extracellular HA, leading to relief of IFP and reopening of otherwise collapsed microvasculature (2,21). The improvement of vascular function was captured by DCE-MRI through the K^{trans} metric. Indeed, K^{trans} elevation was detected as early as 24 hours after a single injection of PEGPH20 (Fig 2), after repeated weekly injection (SI Fig 1), as well as after three combined (PEGPH20 + Gem) treatments (Fig 2). Increase of K^{trans} was corroborated with reductions of tumor HA level in all three, HA-accumulating PDA models, including autochthonous, orthotopic and xenograft model. Taken together, the effects of PEGPH20 and treatment-induced DCE-MRI changes were robustly achieved in a variety of stroma-dense tumors. This observation bolsters confidence that the technique may demonstrate applicability in human trials as well. In clinical trials of PEGPH20, the patients' HA status of the tumor was assessed by endoscopic ultrasound guided biopsy, which cannot sample the entire tumor and is limited in robustness. Validation of DCE-MRI marker would provide a non-invasive, quantitative approach to evaluate the stromal HA level of the entire tumor mass.

K^{trans} represents the combined contribution of vascular permeability and perfusion instead of measuring one or the other. This feature is inherent with K^{trans} obtained using FDA-approved small molecule Gd-contrast agents. For K^{trans} as a stromal marker, this feature could increase the sensitivity since microvascular permeability and perfusion were both increased after stromal intervention (3). DCE-MRI studies with quantitative endpoints are being evaluated in multi-center clinical trials of other cancers, such as prostate and breast cancer (31–34). Quantitative DCE-MRI in human abdominal applications including PDA will be facilitated by motion-robust, rapid imaging techniques and their feasibility in the clinic has been shown (35–37). A standardized clinical DCE-MRI protocol (38) is expected to help control data variability across centers. In conclusion, the proof-of-the-concept study has shown that DCE-MRI is a sensitive and robust quantitative tool for evaluating stroma-directed inventions in preclinical PDA models, and the data support its further evaluation in clinical trials.

Supplementary Material

Refer to Web version on PubMed Central for supplementary material.

Acknowledgments:

We thank Dr. Hee Kwon Song for insightful discussions. This study was partially supported by R21CA198563, R01CA211337 and U24CA231858. All MRI studies were performed in the Small Animal Imaging Facility at the University of Pennsylvania which is supported by the Abramson Cancer Center (P30-CA-016520). Jianbo Cao is grateful for the financial support from the China Scholarship Council (No. 201606310135).

Financial support: This study was partially supported by R21CA198563, R01CA211337 and U24CA231858. All MRI studies were performed in the Small Animal Imaging Facility at the University of Pennsylvania which is supported by the Abramson Cancer Center (P30-CA-016520). Jianbo Cao is grateful for the financial support from the China Scholarship Council (No. 201606310135).

References:

1. Rahib L, Smith BD, Aizenberg R, Rosenzweig AB, Fleshman JM, Matrisian LM. Projecting cancer incidence and deaths to 2030: the unexpected burden of thyroid, liver, and pancreas cancers in the United States. Cancer Res 2014;74(11):2913–21. [PubMed: 24840647]

2. Provenzano PP, Hingorani SR. Hyaluronan, fluid pressure, and stromal resistance in pancreas cancer. Br J Cancer 2013;108(1):1–8. [PubMed: 23299539]

3. Jacobetz MA, Chan DS, Neesse A, Bapiro TE, Cook N, Frese KK, et al. Hyaluronan impairs vascular function and drug delivery in a mouse model of pancreatic cancer. Gut 2013;62(1):112–20. [PubMed: 22466618]

4. Park MS, Klotz E, Kim MJ, Song SY, Park SW, Cha SW, et al. Perfusion CT: noninvasive surrogate marker for stratification of pancreatic cancer response to concurrent chemo- and radiation therapy. Radiology 2009;250(1):110–7. [PubMed: 18984781]

5. Ma W, Li N, Zhao W, Ren J, Wei M, Yang Y, et al. Apparent Diffusion Coefficient and Dynamic Contrast-Enhanced Magnetic Resonance Imaging in Pancreatic Cancer: Characteristics and Correlation With Histopathologic Parameters. Journal of computer assisted tomography 2016;40(5): 709–16. [PubMed: 27224231]

6. Feig C, Gopinathan A, Neesse A, Chan DS, Cook N, Tuveson DA. The pancreas cancer microenvironment. Clin Cancer Res 2012;18(16):4266–76. [PubMed: 22896693]

7. Shepard HM. Breaching the Castle Walls: Hyaluronan Depletion as a Therapeutic Approach to Cancer Therapy. Frontiers in oncology 2015;5(192).

8. Beatty GL. Macrophage-based immunotherapy for the treatment of pancreatic ductal adenocarcinoma. OncoImmunology 2013;2(12):e26837. [PubMed: 24501687]

9. O'Connor JP, Jackson A, Parker GJ, Roberts C, Jayson GC. Dynamic contrast-enhanced MRI in clinical trials of antivascular therapies. Nature reviews Clinical oncology 2012;9(3):167–77.

10. Hingorani SR, Harris WP, Beck JT, Berdov BA, Wagner SA, Pshevlotsky EM, et al. Phase Ib Study of PEGylated Recombinant Human Hyaluronidase and Gemcitabine in Patients with Advanced Pancreatic Cancer. Clin Cancer Res 2016;22(12):2848–54. [PubMed: 26813359]

11. Infante JR, Korn RL, Rosen LS, LoRusso P, Dychter SS, Zhu J, et al. Phase 1 trials of PEGylated recombinant human hyaluronidase PH20 in patients with advanced solid tumours. Br J Cancer 2018;118(2):153–61. [PubMed: 28949957]

12. Hingorani SR, Zheng L, Bullock AJ, Seery TE, Harris WP, Sigal DS, et al. HALO 202: Randomized Phase II Study of PEGPH20 Plus Nab-Paclitaxel/Gemcitabine Versus Nab-Paclitaxel/ Gemcitabine in Patients With Untreated, Metastatic Pancreatic Ductal Adenocarcinoma. J Clin Oncol 2018;36(4):359–66. [PubMed: 29232172]

13. Hingorani SR, Petricoin EF, Maitra A, Rajapakse V, King C, Jacobetz MA, et al. Preinvasive and invasive ductal pancreatic cancer and its early detection in the mouse. Cancer Cell 2003;4(6):437–50. [PubMed: 14706336]

14. Lo A, Wang LC, Scholler J, Monslow J, Avery D, Newick K, et al. Tumor-Promoting Desmoplasia Is Disrupted by Depleting FAP-Expressing Stromal Cells. Cancer Res 2015;75(14):2800–10. [PubMed: 25979873]

15. Zhou R, Pickup S, Yankeelov TE, Springer CS, Jr., Glickson JD. Simultaneous measurement of arterial input function and tumor pharmacokinetics in mice by dynamic contrast enhanced imaging: effects of transcytolemmal water exchange. Magn Reson Med 2004;52(2):248–57. [PubMed: 15282806]

16. Pickup S, Wood AK, Kundel HL. A novel method for analysis of TOROM data. J Magn Reson Imaging 2004;19(4):508–12. [PubMed: 15065176]

17. Pickup S, Zhou R, Glickson JD. MRI estimation of the arterial input function in mice. Academic Radiology 2003;10:963–68. [PubMed: 13678084]

18. Li X, Rooney WD, Springer CS, Jr. A unified magnetic resonance imaging pharmacokinetic theory: intravascular and extracellular contrast reagents. Magn Reson Med 2005;54(6):1351–9. [PubMed: 16247739]

19. Jadin L, Huang L, Wei G, Zhao Q, Gelb AB, Frost GI, et al. Characterization of a novel recombinant hyaluronan binding protein for tissue hyaluronan detection. Journal of Histochemistry & Cytochemistry 2014;62(9):672–83. [PubMed: 24891594]

20. Milane L, Duan Z, Amiji M. Pharmacokinetics and biodistribution of lonidamine/paclitaxel loaded, EGFR-targeted nanoparticles in an orthotopic animal model of multi-drug resistant breast cancer. Nanomedicine: Nanotechnology, Biology and Medicine 2011;7(4):435–44.

21. Provenzano PP, Cuevas C, Chang AE, Goel VK, Von Hoff DD, Hingorani SR. Enzymatic targeting of the stroma ablates physical barriers to treatment of pancreatic ductal adenocarcinoma. Cancer Cell 2012;21(3):418–29. [PubMed: 22439937]
22. Thompson CB, Shepard HM, O'Connor PM, Kadhim S, Jiang P, Osgood RJ, et al. Enzymatic depletion of tumor hyaluronan induces antitumor responses in preclinical animal models. Mol Cancer Ther 2010;9(11):3052–64. [PubMed: 20978165]
23. Gore J, Korc M. Pancreatic Cancer Stroma: Friend or Foe? Cancer Cell 2014;25(6):711–12. [PubMed: 24937454]
24. Sherman Mara H, Yu Ruth T, Engle Dannielle D, Ding N, Atkins Annette R, Tiriac H, et al. Vitamin D Receptor-Mediated Stromal Reprogramming Suppresses Pancreatitis and Enhances Pancreatic Cancer Therapy. Cell 2014;159(1):80–93. [PubMed: 25259922]
25. Olive KP, Jacobetz MA, Davidson CJ, Gopinathan A, McIntyre D, Honess D, et al. Inhibition of Hedgehog signaling enhances delivery of chemotherapy in a mouse model of pancreatic cancer. Science 2009;324(5933):1457–61. [PubMed: 19460966]
26. Catenacci DV, Junttila MR, Karrison T, Bahary N, Horiba MN, Nattam SR, et al. Randomized Phase Ib/II Study of Gemcitabine Plus Placebo or Vismodegib, a Hedgehog Pathway Inhibitor, in Patients With Metastatic Pancreatic Cancer. J Clin Oncol 2015;33(36):4284–92. [PubMed: 26527777]
27. Beatty GL, Chiorean EG, Fishman MP, Saboury B, Teitelbaum UR, Sun W, et al. CD40 agonists alter tumor stroma and show efficacy against pancreatic carcinoma in mice and humans. Science 2011;331(6024):1612–6. [PubMed: 21436454]
28. Froeling FE, Kocher HM. Homeostatic restoration of desmoplastic stroma rather than its ablation slows pancreatic cancer progression. Gastroenterology 2015;148(4):849–50. [PubMed: 25724458]
29. DelGiorno Kathleen E, Carlson Markus A, Osgood R, Provenzano Paolo P, Brockenbough JS, Thompson Curtis B, et al. Response to Chauhan et al.: Interstitial Pressure and Vascular Collapse in Pancreas Cancer - Fluids and Solids, Measurement and Meaning. Cancer Cell 2014;26(1):16–17. [PubMed: 25026210]
30. Akisik MF, Sandrasegaran K, Bu G, Lin C, Hutchins GD, Chiorean EG. Pancreatic Cancer: Utility of Dynamic Contrast-enhanced MR Imaging in Assessment of Antiangiogenic Therapy. Radiology 2010;256(2):441–49. [PubMed: 20515976]
31. Huang W, Chen Y, Fedorov A, Li X, Jajamovich GH, Malyarenko DI, et al. The Impact of Arterial Input Function Determination Variations on Prostate Dynamic Contrast-Enhanced Magnetic Resonance Imaging Pharmacokinetic Modeling: A Multicenter Data Analysis Challenge. Tomography: a journal for imaging research 2016;2(1):56–66.
32. Huang W, Li X, Chen Y, Li X, Chang MC, Oborski MJ, et al. Variations of Dynamic Contrast-Enhanced Magnetic Resonance Imaging in Evaluation of Breast Cancer Therapy Response: A Multicenter Data Analysis Challenge. Translational oncology 2014;7(1):153–66. [PubMed: 24772219]
33. Head Joint and Neck Radiotherapy MRI Development Cooperative. A Multi-Institutional Comparison of Dynamic Contrast-Enhanced Magnetic Resonance I maging Parameter Calculations. Scientific reports 2017;7(1):11185.
34. Sorace AG, Partridge SC, Li X, Virostko J, Barnes SL, Hippe DS, et al. Distinguishing benign and malignant breast tumors: preliminary comparison of kinetic modeling approaches using multi-institutional dynamic contrast-enhanced MRI data from the International Breast MR Consortium 6883 trial. Journal of medical imaging (Bellingham, Wash) 2018;5(1):011019.
35. Benkert T, Feng L, Sodickson DK, Chandarana H, Block KT. Free-breathing volumetric fat/water separation by combining radial sampling, compressed sensing, and parallel imaging. Magn Reson Med 2017;78(2):565–76. [PubMed: 27612300]
36. Seo N, Park SJ, Kim B, Lee CK, Huh J, Kim JK, et al. Feasibility of free-breathing dynamic contrast-enhanced MRI of the abdomen: a comparison between CAIPIRINHA-VIBE, Radial-VIBE with KWIC reconstruction and conventional VIBE. Br J Radiol 2016;89(1066):20160150.
37. Lin W, Guo J, Rosen MA, Song HK. Respiratory motion-compensated radial dynamic contrast-enhanced (DCE)-MRI of chest and abdominal lesions. Magn Reson Med 2008;60(5):1135–46. [PubMed: 18956465]

38. Profile: DCE MRI Quantification. by RSNA QIBA DCE-MRI Committee 2011:http://www.rsna.org/uploadedFiles/RSNA/Content/Science_and_Education/QIBA/DCE-MRI_Quantification_Profile_v1%200-ReviewedDraft%08-8-12.pdf.

Statement of translational relevance:

Using relevant animal models, this study demonstrated that a quantitative marker derived from dynamic contrast enhance MRI can detect early responses to stroma-directed drug for pancreatic ductal adenocarcinoma with a high level of hyaluronan. This imaging tool has the potential to non-invasively evaluate the stromal hyaluronan level of the entire tumor mass.

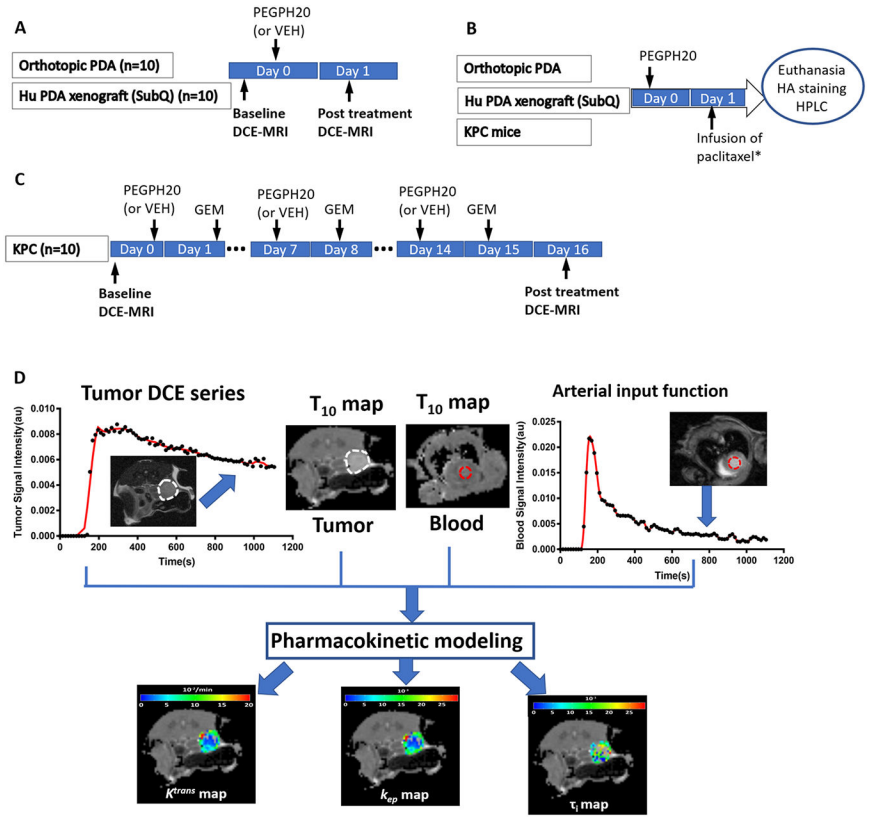

Figure 1. Treatment, imaging and assay protocol.

A: Orthotopic and xenograft PDA models received one single injection of PEGPH20 (or vehicle) and DCE-MRI was performed before and 24 h post treatment. B: All three models received one single treatment of PEGPH20 (or VEH) and 24 h later, tumors were harvested for HA staining. * Only the orthotopic model was infused with paclitaxel 2 h before euthanasia to assess drug delivery to the tumor by HPLC detection of paclitaxel in tumor homogenate (see Methods). C: KPC model received 3 treatments of PEG20 followed by gemcitabine (GEM) the next day, and MRI was performed at baseline and post treatment. The number of mice was shown in parentheses. D: DCE-MRI acquisition and processing

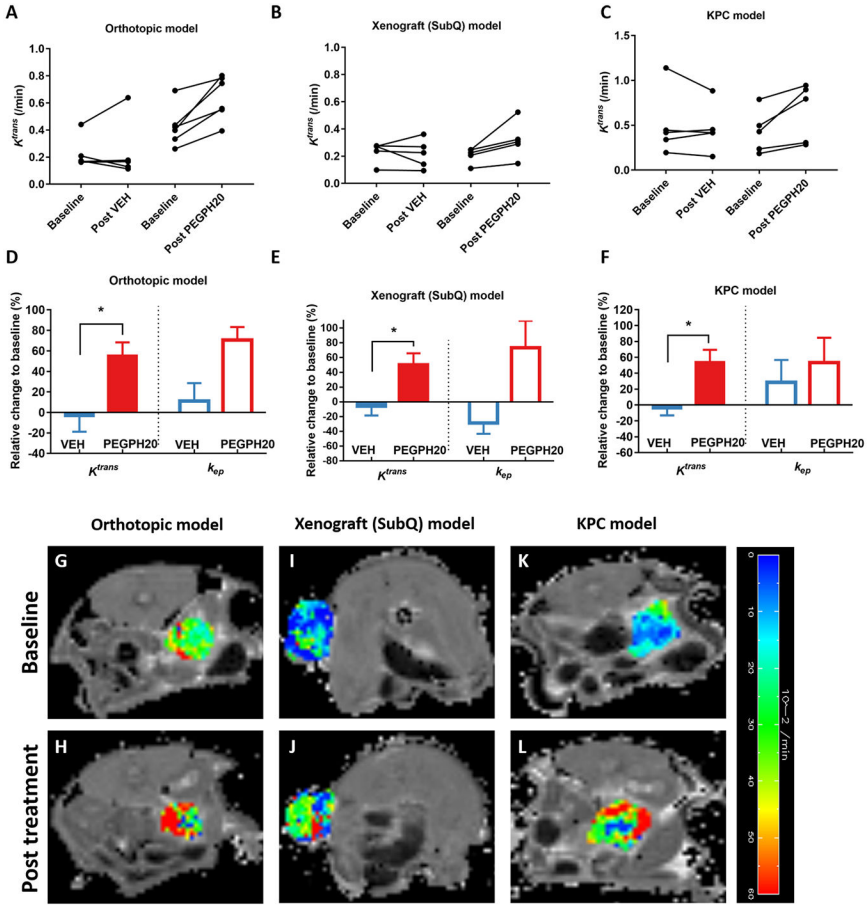

Figure 2. DCE-MRI detects responses to stroma-directed intervention (PEGPH20) in all three PDA models.

Paired K^{trans} values from orthotopic model (**A**) and (**B**) human xenograft before and after a single injection of PEGPH20 or VEH, as well as from KPC mice at baseline and post-three treatments of PEGPH20 plus gemcitabine (**C**). Percent changes of K^{trans} and k_{ep} after the treatment from baseline (**D-F**). Baseline and post-treatment K^{trans} map of the tumor (in color scale) overlaid on the respective T_{10} map (in grey scale, **G-L**). ***:** P< 0.05 compared to VEH group (Mann-Whitney U test).

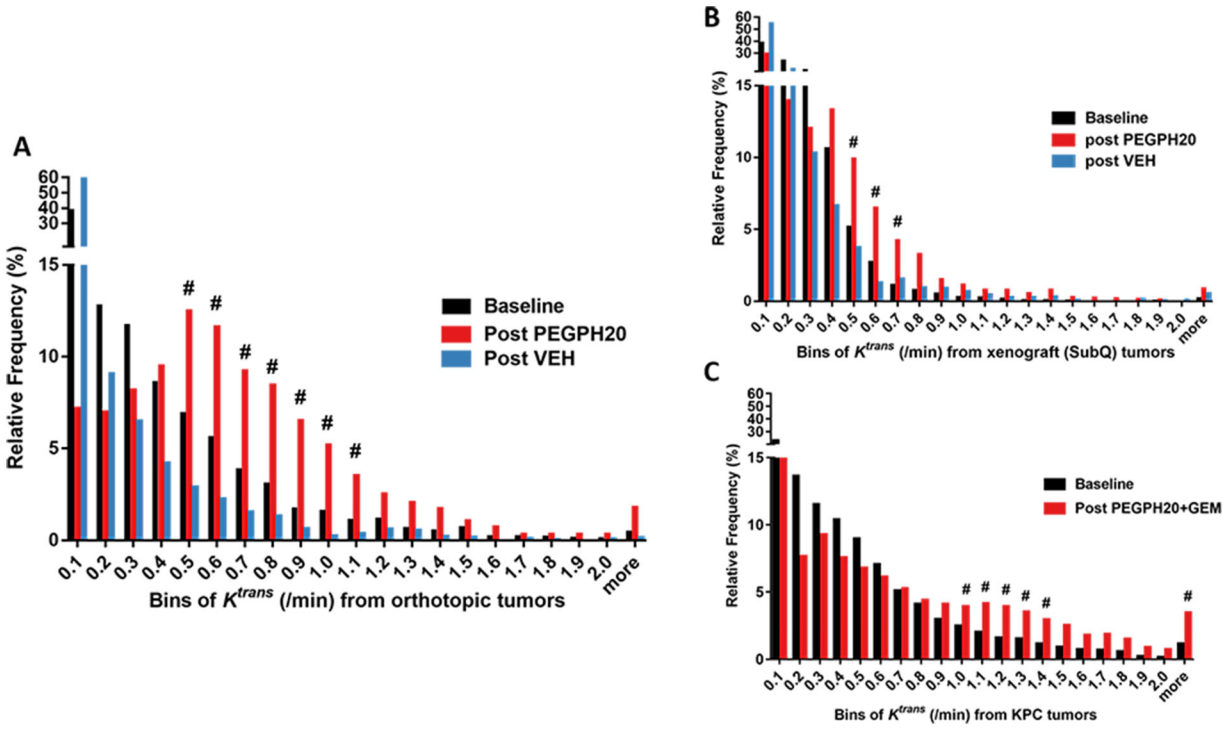

Figure 3. Histograms of K^{trans} distribution at baseline, after single PEGPH20 or VEH treatment in orthotopic (A) and xenograft (B) model.

Baseline and post-combined treatment for the KPC model (**C**). Treatment and imaging schedules are the same as in Fig 2. In A and B, the baseline histogram (black) is pooled from baseline K^{trans} values of both treatment groups, whereas in C, K^{trans} values at baseline and post-treatment of PEGPH20+GEM group were analyzed (the control group was not plotted due to small n). # marks bins whose frequency is ≥1% and had an increase of ≥ 50% compared to baseline.

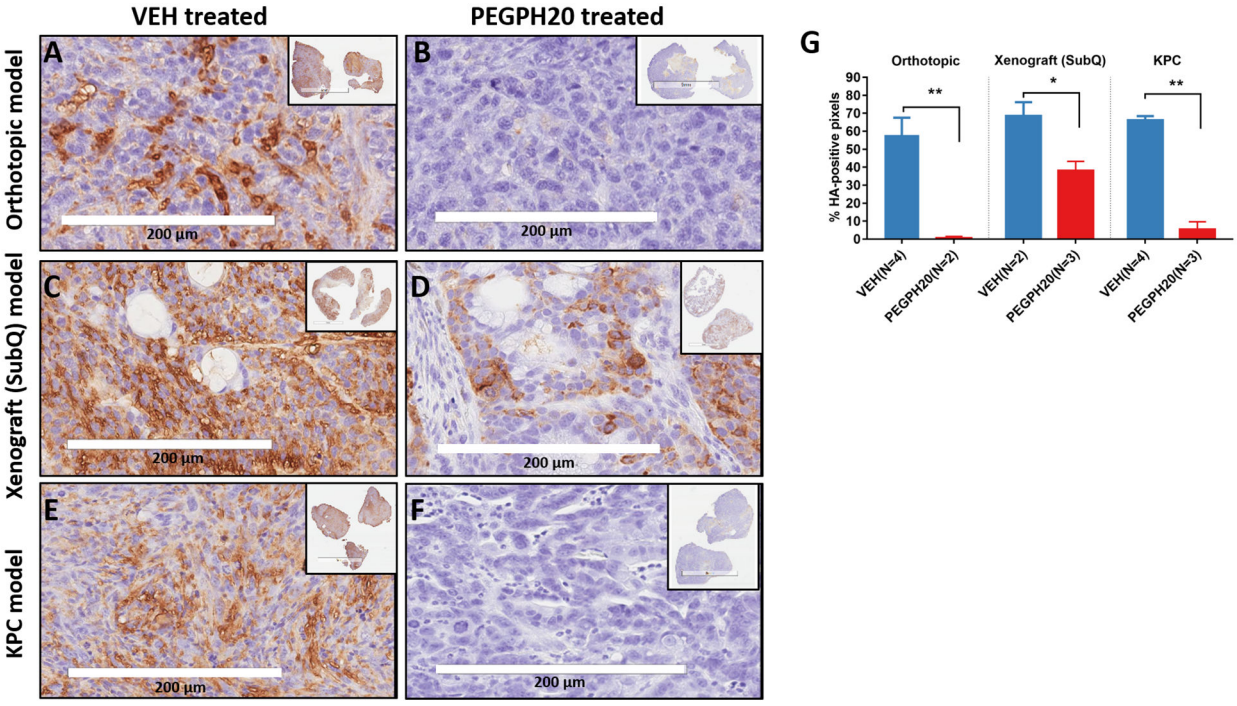

Figure 4. Tumor hyaluronan level and drug delivery efficiency in response to PEGPH20 or VEH treatment.

Representative micrographs of immunostaining for hyaluronan in tumor sections obtained from VEH or PEGPH20 treated KPC model (**A, B**) orthotopic model (**C, D**) and xenograft model (**E, F**). The percentage (mean +/− SD) of hyaluronan-positive pixels in three models after VEH or PEGPH20 treatment (**G**). *: P< 0.05, **: P<0.005, compared to the respective VEH group. Treatment/imaging schedules are the same as in Fig 1A.

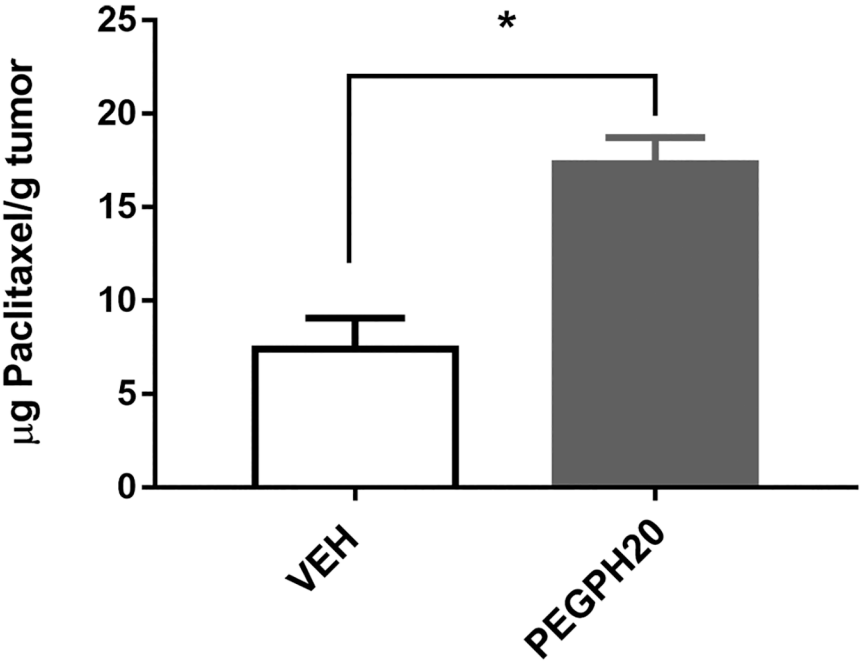

Figure 5. PEGPH20 treatment increased chemotherapy drug (paclitaxel) penetration to the tumor.

Content of paclitaxel accumulated in the orthotopic tumor after PEGPH20 (n=3) or VEH treatment (n=3). *: P< 0.05 compared to the respective VEH group. Treatment/imaging schedules are the same as in Fig 1A.